Negative thermal expansion of cubic silicon dicarbodiimide, $Si(NCN)_2$, studied by ab initio lattice dynamics

Li Li

College of Physics, Sichuan University, Chengdu, Sichuan 610065, People's Republic of China, and
College of Computer Science and Technology, Civil Aviation Flight University of China, 46 Nanchang Road, Guanghan, Sichuan, 618307, People's Republic of China

Sijie Zhang

College of Physics, Sichuan University, Chengdu, Sichuan 610065, People's Republic of China.

Keith Refson

Department of Physics, Royal Holloway University of London, Egham Hill, Egham, Surrey, TW20 0EX, United Kingdom.

Martin T Dove

College of Computer Science, Sichuan University, Chengdu, Sichuan 610065, People's Republic of China, and
Department of Physics, School of Sciences, Wuhan University of Technology, 205 Luoshi Road, Hongshan district, Wuhan, Hubei 430070, People's Republic of China.

E-mail: martin.dove@icloud.com

Abstract. We report an ab initio calculation of crystal structure and lattice dynamics of cubic silicon dicarbodiimide, $Si(NCN)_2$, using Density Functional Theory methods. The calculations reveal a low-energy spectrum of Rigid Unit Modes that are shown to be associate with negative thermal expansion. Comparisons are drawn with the closely-related NTE material $Zn(CN)_2$, the related cubic-cristobalite phase of SiO_2.

1. Introduction

Interest in negative thermal expansion (NTE) has grown significantly over the past two decades as we have seen new materials that exhibit this counter-intuitive physical property. The early materials, as discussed in some earlier [1, 2, 3, 4] and more recent reviews [5, 6, 7, 8, 9], typically had formulae of the form MX_2O_7, MX_2O_8 and $M_2X_3O_{12}$. The crystal structures of these materials formed as infinite networks of corner-linked

MO_6 octahedra and XO_4 tetrahedra. Since the early days NTE has been found in a wide range of materials. Actually simultaneously with the re-discovery of NTE in ZrW_2O_8 [10, 11] that ushered in the current interest was the discovery of NTE in zeolitic materials of formula SiO_2 or $AlPO_4$ [12, 13, 14, 15, 16, 17, 18]. These materials consist of corner linked tetrahedra, as also do quartz and cristobalite forms of silica in their high-temperatures phases [19, 20, 21]. More recently NTE was found in the simple cubic form of ScF_3 [22], which consists only of corner-linked ScF_6 octahedra.

The natural development after the work on the pure oxides (and halide analogues) was to investigate materials in which the linker oxygen atoms are replaced by small molecular ions. The simples analogues of ScF_3 (linked octahedra) and SiO_2 (linked tetrahedra) are obtained by replacing the oxygen by cyanide anions, and indeed NTE is found in the respective materials of the Prussian blue family [23, 24, 25, 26] and $Zn(CN)_2$ and related materials [27, 28, 28, 29, 30]. There is great interest in extending the range of potential molecular ions in such materials, particularly if they can lead to enhanced NTE in the way demonstrated by $Zn(CN)_2$ [27].

In this paper we consider the new material silicon dicarbodiimide, $Si(NCN)_2$ [31, 32], which in its high-temperature β-phase has a similar crystal structure to that of $Zn(CN)_2$ but with the extended NCN^{2-} anion replacing the CN^- anion, Figure 1. There is some discussion regarding whether the crystal structure represented with linear Si–N–C–N–Si atomic connections is an idealisation of the true structure [31, 32, 33, 34], with the possibility that there are local bond-bending fluctuations, reminiscent of the dynamic disorder in the cubic phase of cristobalite [35, 36, 37, 38, 39]. The crystal structure of the low-temperature α-phase appears not to have been deduced experimentally, but has been investigated using ab initio methods [40].

The same researchers discovered that the cubic β-phase of $Si(NCN)_2$ shows negative thermal expansion [33], with coefficients of volume expansivity α_V in the range -3.7 to -5.8 MK^{-1} (the paper actually reports data for linear rather than volume expansivity). This is somewhat smaller than for most other NTE materials as tabulated in the review of Dove and Fang [8], and in particular smaller by an order of magnitude than in $Zn(CN)_2$ [27]. However, ab initio simulation methods reported in the same paper showed a rather larger negative volume expansivity of $\alpha_V = -60 \pm 9$ MK^{-1}, which is comparable to that of $Zn(CN)_2$. Faced with a choice between finding fault with the experiment or simulation, the authors were inclined to put more trust in their simulation, and they suggested that the experimental samples may have suffered from small-size effects and impurities.

In this paper we examine the NTE in $Si(NCN)_2$ using ab initio lattice dynamics methods, using methods similar to those used to evaluate NTE in Cu_2O [41], $Zn(CN)_2$ [42], $Y_2W_3O_{12}$ [43], ZrW_2O_8 and MOF-5 [44]. The results form an interesting comparison with the results of $Zn(CN)_2$ [42] in terms of the underlying flexibility of the network. The results are analysed in terms of the Rigid Unit Modes (RUMs) of the system [45, 46, 47], in which the network flexibility can be described in terms of the translation and rotation models of 'rigid' SiN_4 tetrahedra connected by 'rigid' NCN rods. The RUM model does

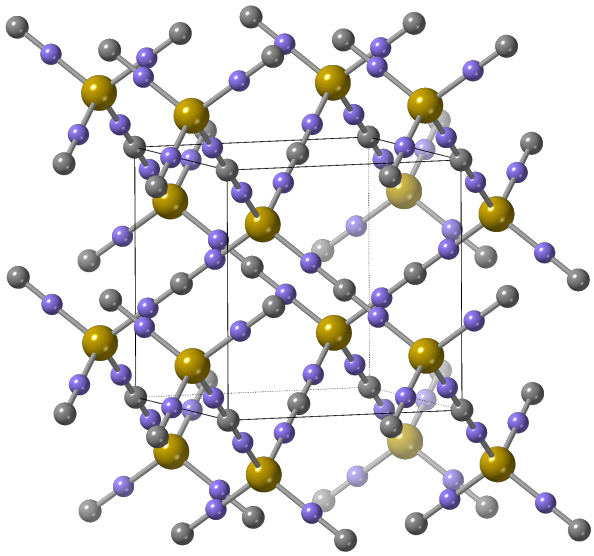

Figure 1. Crystal structure of the cubic phase of $Si(NCN)_2$, from the paper of Riedel et al [31]. The crystal has space group $Pn\bar{3}m$, with lattice parameter $a = 6.19$ Å. It consists of two interpenetrating networks of SiN_4 tetrahedra linked by the NCN^{2-} anions.

not presume infinite rigidity of the structural units, but highlights the differentiation of stiffer and weaker forces, the latter being the flexing of the Si–N–C angle, as previously indicated as having a wide variation from linear from consideration of bond lengths and from the NMR [31, 40, 33, 34]. The issue of rigidity has been discussed in general detail elsewhere [48]. We also use the ab initio lattice dynamics calculations to give information of the instability of the cubic β-phase that leads to the phase transition to the lower-symmetry α-phase [31, 33].

2. Simulation methods

The ab initio calculations reported here were performed using the CASTEP software package [49], version 19.1. CASTEP is an implementation of the standard density functional theory (DFT) methods, using plane waves to represent the electron wave functions represented, and CASTEP's internal pseudopotentials to represent the effects of the core electrons. The GGA-PBE functional [50, 51] was used for all calculations, with norm-conserving pseudopoentials. A plane-wave cutoff energy of 1200 eV was used, together with a Monkhorst-Pack grid [52] for wave vectors of size $8 \times 8 \times 8$ for integration of electronic states. The material was constrained as an insulator. Forces and stresses within the geometry optimisations were performed to convergence of XXX eV/Å and 10^{-4} GPa respectively.

Phonon frequencies were calculated using the density functional perturbation theory (DFPT) method [53, 54]. For phonon dispersion curves along high-symmetry directions in reciprocal space, a Monkhorst-Pack grid of size $8 \times 8 \times 8$ was used for calculations

Table 1. Comparison of the observed crystal structure [31] and selected bond lengths of Si(NCN)$_2$ with those calculated from a zero-pressure optimisation and with a small expansion. The crystal structure has space group $Pn\bar{3}m$, with origin at the centre of symmetry (co-located with the position of the C atom, site symmetry $\bar{3}m$). In this setting Si has fractional coordinates $1/4, 1/4, 1/4$, C has fractional coordinations $0, 0, 0$, and N has fractional coordinates x, x, x.

	Experimental [31]	Optimised DFT	Expanded DFT
a (Å)	6.1885(1)	6.6998	6.7221
x	0.103(2)	0.1043	0.1042
Si–N (Å)	1.576	1.691	1.698
N–C (Å)	1.104	1.210	1.213

of the dynamical matrix, and phonon frequencies for specific wave vectors along the line calculatied by interpolation. A convergence tolerance for force constants during the DFPT calculations of 10^{-5} eV/Å^2 was used. The phonon acoustic sum rule was enforced. For calculation of thermodynamic properties phonon frequencies were calculated for a set of random wave vectors.

3. Crystal structure and lattice dynamics of β-Si(NCN)$_2$

The relaxed crystal structure optimised at zero pressure is shown in Table 1, where it is compared with the experimental crystal structure [31]. The striking difference is that the Si–N and N–C bond lengths are overestimated from the experimental values by 7% and 10% respectively, leading to an overestimate of the unit cell parameter by 8%. This discrepancy is not typical of the accuracy of DFT. However, we note that our value of the carbodiimide N–C bond length is typical of those found in other materials. For example, the four distinct N–C bond lengths in BaZn(NCN)$_2$ are found from x-ray diffraction measurements and by DFT calculations to be around 1.22 Å and 1.23 Å respectively, consistent with our calculated values [55]. The discrepancy between the DFT and experimental distances seen here in β-Si(NCN)$_2$ quite likely reflect the effect of thermal motion that involves rotations of rigid bonds, as indeed was pointed out when the crystal structure was determined [31]. This is very similar to the situation in the related material β-cristobalite [36, 37] and indeed in the case of the better known quartz polymorph of silica [56, 57]. We will discuss this point in more detail below.

Calculations of the phonon dispersion curves for the optimised structure (we will discuss the phonon dispersion relations in more detail below) showed that for all wave vectors along the main symmetry directions up to eight branches have negative eigenvalues of the dynamical matrix, indicating an inherent instability. Given that we know there is a phase transition to a structure of lower (but so far undetermined), the calculation of some unstable vibrations is not surprising. We can drive the eigenvalues towards positive values by a slight expansion of the lattice, and we report in Table 1 the crystal structure for a specific fixed lattice parameter at which the low-frequency

Table 2. Vibration frequencies for zero wave vector calculated for the expanded unit cell reported in Table 1, given in two units for convenience. The mode decomposition is $A_{2u} + E_u$ (acoustic models) and $A_{1g} + E_g + 4T_g + 4A_{2u} + 2B_{2u} + 6E_u + 2T_u$ (optic modes). The symbols R and IR indicated Raman and infrared activity.

A_{1g} (R)		$3E_g$ (R)		$4T_g$ (R)			
cm^{-1}	THz	cm^{-1}	THz	cm^{-1}	THz		
1578.6	47.36	241.5	7.24	48.1	1.44		
				224.8	6.75		
				577.3	17.32		
				1582.7	47.48		
$4A_{2u}$ (IR)		$2B_{2u}$ (–)		$6E_u$ (IR)		$2T_u$ (IR)	
cm^{-1}	THz	cm^{-1}	THz	cm^{-1}	THz	cm^{-1}	THz
334.3	10.03	667.7	20.03	219.2	6.58	36.0	1.08
528.8	15.86	2377.6	71.33	301.3	9.04	525.5	15.77
847.9	25.44			524.8	15.75		
2328.5	69.86			533.6	16.01		
				743.4	22.30		
				2202.5	66.07		

modes all have positive eigenvalues.

The calculated frequencies for vibrations with zero wave vector are given in Table 2. At the time of writing there are little in the ways of reported vibrational frequencies for $Si(NCN)_2$ measured by spectroscopy other than from a preliminary characterisation by infrared spectroscopy. That showed the existence of an IR-active mode at a frequency of 2174 cm^{-1}, which is the antisymmetric stretching mode of the N–C–N anion. The corresponding modes are the four highest-frequency modes of the group $A_{2u} + B_{2u} + E_u$, with average of 2303 cm^{-1} (69.1 THz), higher than experiment by 6%. From a tabulation of frequency values [58], the symmetric stretch frequency of a carbodiimide anion is around 1250 cm^{-1}. The calculated mode is of the group $A_{1g} + T_g$, with average of 1581 cm^{-1} (47.4 THz). This is around 25% larger than the value for carbodiimide salts , and we attribute this to a strong Si–N bond that is co-linear with the N–C–N bond, providing a resistance to the motion and hence higher frequency. The same study reports the N–C–N bending frequencies for a range of carbodiimide crystals to have frequencies of around 650 cm^{-1}, in some cases dipping down to 580 cm^{-1}. In the calculations the expected 8 N–C–N bending modes correspond to the $A_{2u} + 2E_u + T_u$ group between 524.8–533.6 cm^{-1} (average around 15.9 THz).

The lower-frequency part of the phonon dispersion curves for the expanded lattice with parameters in Table 1 – that is, the range excluding the high-frequency symmetric and antisymmetric stretch modes – are shown for the main symmetry directions in Figure 2. The phonon density of states sampled from across the whole Brillouin zone is shown in Figure 3.

From the slopes of the acoustic mode dispersion curves we calculated values of

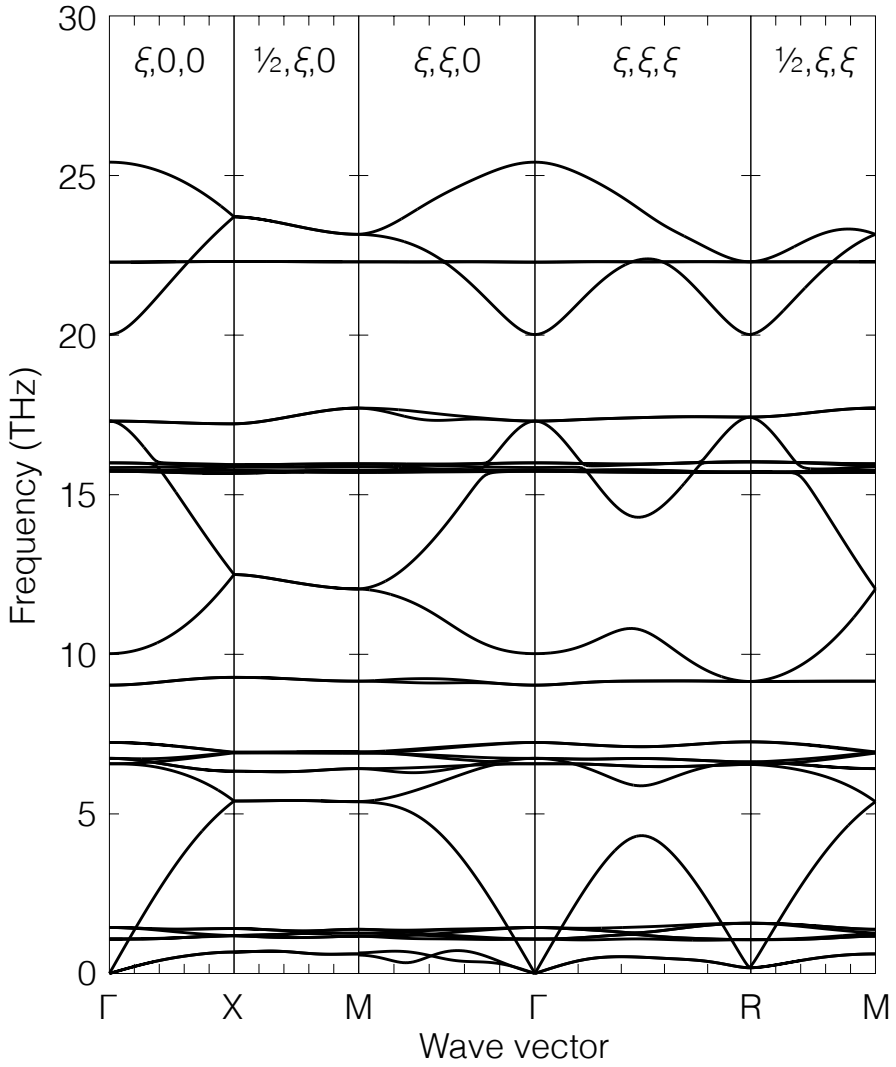

Figure 2. Calculated phonon dispersion curves for the structure of cubic Si(NCN)$_2$ with the expanded lattice parameter of Table 1. Results are shown for wave vectors along the high-symmetry directions in reciprocal space. In order to provide clarity for the lower frequency results we exclude the high-frequency symmetric and antisymmetric stretch frequencies of 47 and 69 THz respectively.

the elastic constants for the expanded lattice of C_{11} = 102 GPa, C_{12} = 96 GPa, and C_{44} = 2.8 GPa, yielding a value for the bulk modulus of 98 GPa. The values of C_{44} are particularly sensitive to the size of the lattice parameter, and for the equilibrium lattice parameter reported in Table 1 the transverse acoustic modes are systematically unstable and C_{44} has a negative value. Furthermore, we consider that the true value of these modulii at high temperatures will be considerably lower than these values for this reason. In the ordered structure, compression will exert forces along the linear Si–N–C–N–Si linkage, which will compress relatively rigid bonds giving a relatively high elastic modulus. On the other hand, at high temperature the atomic displacements will crumple this linkage, and compressional forces can be readily absorbed by further

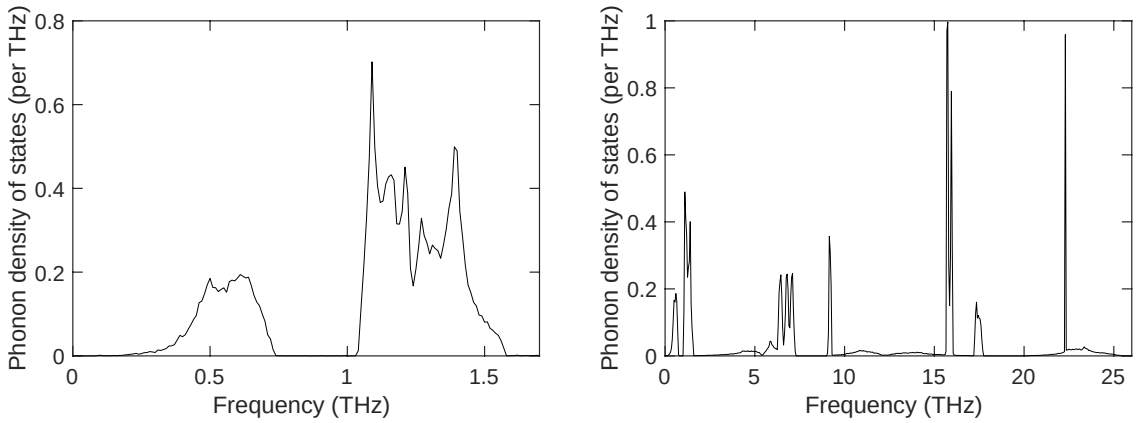

Figure 3. Calculated phonon density of states for the structure of cubic Si(NCN)$_2$ with the expanded lattice parameter of Table 1, excluding the higher frequency range that includes the symmetric and anti-symmetric stretch modes of the N–C–N anion. The diagram on the left shows in more detail the low-frequency part of the density of states, highlighting the region containing the Rigid Unit Modes. Note that the histogram bin is five times wider in the wide-range plot on the right in order to reduce the heights of the higher-frequency peaks; this accounts for the difference in the heights of the common parts of the density of states in the two diagrams.

crumpling rather than by compression of the bonds. This point has been discussed with regard to the phenomenon of pressure-induced softening as found in Zn(CN)$_2$ [42, 59] and predicted to be a more general phenomenon [60, 61].

4. Rigid Unit Modes and network flexibility of β-Si(NCN)$_2$

The RUM analysis performed for Zn(CN)$_2$ by Goodwin [62] is directly applicable to β-Si(NCN)$_2$ since the crystal structures both consist of two interpenetrating cristobalite networks in a crystal structure of cubic symmetry with linear cation–anion–cation connectivities. It was shown that there are eight RUMs per wave vector, with two corresponding to the transverse acoustic modes, three corresponding to modes in which there is a uniform displacement of the N–C–N anion from the corresponding Si...Si vector, and three corresponding to modes in which the N–C–N anion rotates about the position of the C atom to give a twist to the Si–N–C–N–Si vector. Inspection of the phonon eigenvectors showed that the displacement modes at zero wave vector correspond to the T_u mode of frequency 1.08 THz, and the twist modes at zero wave vector correspond to the T_g mode of frequency 1.44 THz. Thus we conclude that the optic-mode RUMs in Si(NCN)$_2$ are systematically the lowest-frequency modes. Inspection of the phonon density of states shown in Figure 3 indicates that the transverse acoustic RUMs are the spectrum between 0–0.8 THz, and the optic-mode RUMs are the spectrum between 1–1.6 THz. There is a significant gap before reaching the lower frequency of the other optic phonons at just over 5 THz.

It is interesting to compare the RUMs in Si(NCN)$_2$ with those in Zn(CN)$_2$, as

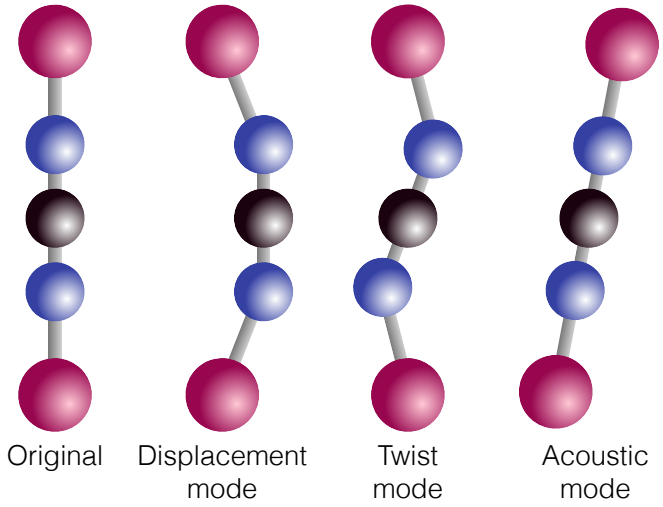

Figure 4. The three types of Rigid Unit Mode – displacement mode, twist mode, and acoustic mode – compared with the original crystallographic arrangement. All three RUMs pull the Si atoms towards each other in the vertical direction. The end atoms are the Si cations, between which are the carbonodiimide N–C–C anions.

explored in detailed by Fang et al [42]. As we noted before, the crystal structure is topologically equivalent, and the fact that the C–N anion has head-to-tail disorder means that it is effectively a quadrupolar rather dipolar molecular anion, as is the N–C–N anion. However, in $Zn(CN)_2$ there are strong angular forces along the Zn–cyanide–Zn linkage, which push the displacement RUM frequencies up to the range 2–4 THz, and the twist RUM up to frequencies in the range 8.5–9 THz. Thus in $Zn(CN)_2$ the optic RUMs play a very weak role in the NTE in this material, and instead the larger contribution to NTE comes from the acoustic RUMs, whose frequencies are mostly below 1 THz.

From the discussion of phonon instabilities given above, we can note that in the equilibrium structure calculated by DFT, there is an exact correspondence between the unstable phonons and the RUMs. Expansion of the lattice is sufficient to stabilise the RUMs, because the atomic structure is put under some degree of tension. An analogy might be of a guitar string.that vibrations only when a certain tension is applied. In this context, the comparison with the β-cristobalite phase of silica is very pertinent. Our understanding the high-temperature cubic phase is that the RUMs have low-frequency [35] and hence high amplitude, and it was shown that most of the atomic motions can be associated with RUMs in which the SiO_4 tetrahedral move with minimal distortions [38]. As found here, the rotations of the tetrahedra lead to a shortening of the distance between average positions of neighbouring atoms compared to the instantaneous bond lengths [36, 37].

β-$Si(NCN)_2$ has a lot more RUMs than in β-cristobalite, with the RUMs in the latter case restricted to planes of wave vectors in reciprocal space [35, 45, 46, 63]. On this basis, we expect to see large-amplitude thermal motion based on the superposition of all RUMs, and this thermal motion will give rise to the apparent shortening of bonds

(that is, shortening of distance between average atom positions) seen by the comparison of DFT results and experimental structure data.

5. Mode Grüneisen parameters and negative thermal expansion in β-Si(NCN)$_2$

The Grüneisen model for negative thermal expansion, as discussed in some recent reviews [3, 8, 9], is based on the fact that a change in volume will cause a change in the values of phonon frequencies as a result of changes in interatomic bond force constants due to increase separation lengths. The coefficient of volume expansivity is given as

$$\alpha_V = \frac{C_V \overline{\gamma}}{BV} \tag{1}$$

where V is the volume, $B = -V(\partial P/\partial V)_T$ is the isothermal bulk modulus, C_V is the heat capacity, The quantity $\overline{\gamma}$ is the "overall Grüneisen parameters", and this defines how phonon frequencies depend on volume. It is defined as a weighted sum over individual mode Grüneisen parameters:

$$\overline{\gamma} = \frac{1}{C_V} \sum_i c_i \gamma_i \tag{2}$$

where the sum is over all phonon modes, and the mode Grüneisen parameters γ_i are defined as

$$\gamma_i = -\frac{V}{\omega_i} \frac{\partial V}{\partial \omega_i} \tag{3}$$

where ω_i is the frequency of phonon mode i. The coefficients c_i which weight the contribution from each mode are given as

$$c_i = \hbar \omega_i \frac{\partial n(\omega_i, T)}{\partial T} \tag{4}$$

where T is the temperature, and $n(\omega_i, T) = 1/\left(\exp(\hbar\omega_i/k_\mathrm{B}T) - 1\right)$ is the Bose-Einstein distribution. It follows that $C_v = \sum_i c_i$. In most materials $\overline{\gamma} \sim +1$, but in NTE materials $\overline{\gamma}$ must have a negative value, which will typically arise from a material having a sufficient number of individual mode Grüneisen parameters γ_i with large negative values; these will typically be for the lower-frequency modes.

Mode Grüneisen parameters were calculated from the phonons calculated for two very slightly different volumes, using a random selection of wave vectors. The pairs of frequencies to compare were selected on the basis of matching mode eigenvectors, using software described elsewhere [43]. The average values within small ranges of frequencies are shown in Figure 5. From comparison with the density of states, Figure 3, we can see that the RUMs are very closely associated with the modes with negative values of mode Grüneisen parameters, and therefore contribute significantly to NTE. We can see separately in Figure 5 the contributions from the acoustic RUMs (0–0.7 THz) and from the bands of optic RUMS (1–1.6 THz). Although there are other modes with negative values of mode Grüneisen parameters – including the N–C–N bending modes at around

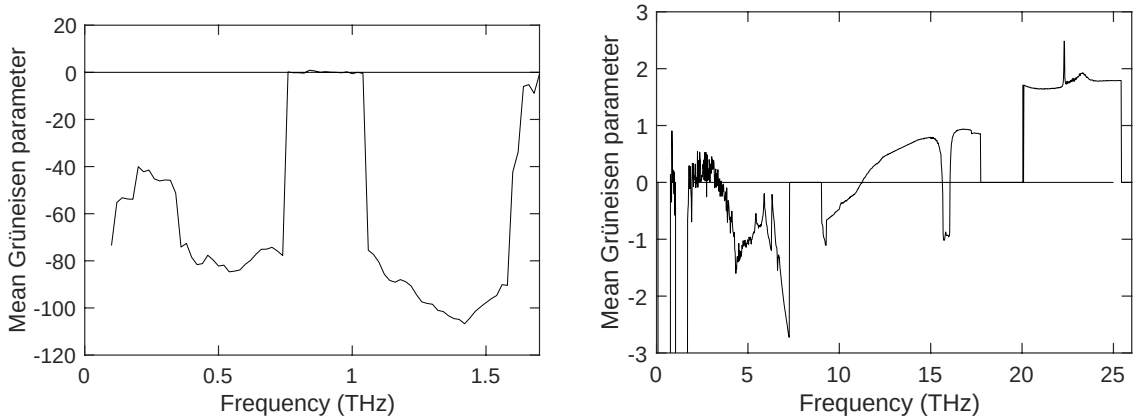

Figure 5. Frequency-ranged average values of the mode Grüneisen parameters plotted over two ranges of frequencies. The averaging interval was 0.02 THz. Data are presented in two ranges of frequency because of the huge negative values at low frequency.

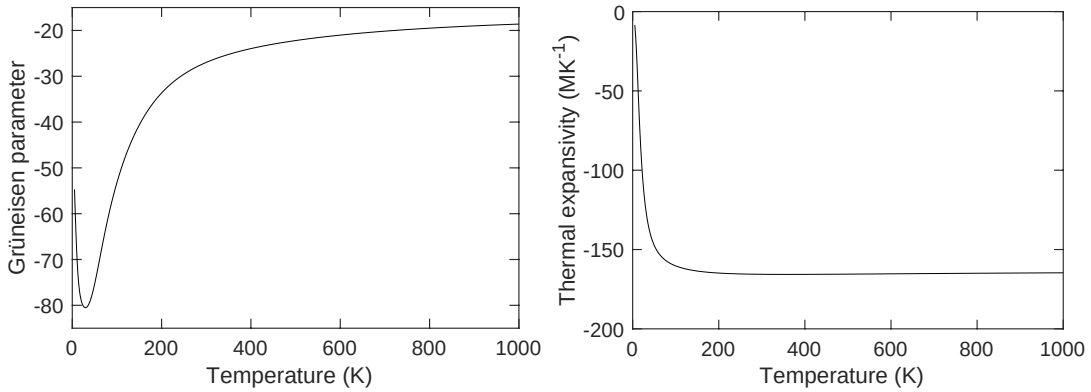

Figure 6. Temperature-dependence of the overall Grüneisen parameter (left) and coefficient of thermal expansion (right).

15.9 THz – the NTE is clealy dominated by the effects of all the RUMs. We note also that as in $Zn(CN)_2$ the acoustic RUMs are important for NTE. The immediate impression Figure 5 that the acoustic RUMs are roughly of equivalent importance for NTE as the optic-mode RUMs. The same was found for Cu_2O [41] and MOF-5 [44].

Figure 6 shows the calculated values of the overall Grüneisen parameter and coefficient of thermal expansivity as functions of temperature for the expanded lattice of Table 1. The value of the coefficient of thermal expansivity is considerably larger (more negative) than reported from ab initio molecular dynamics [33], which in turn is larger than the experimental value as discussed above.

One way to try to account for the discrepancy between the values of thermal expansivity of the previous MD [33] and our calculation is to return to the definition of the mode Grüneisen parameters and write then in the alternative but equivalent form

$$\gamma_i = -\frac{V}{2\omega_i^2}\frac{\partial\omega^2}{\partial V} \tag{5}$$

which as the advantage of emphasising that the solutions of the dynamical matrix are the values ω_i^2. Linearising the variation of force constant on change in volume as $\Delta\omega_i^2 = \omega_i^2 + (\partial\omega_i^2/\partial V)\,\Delta V$ if follows that $\gamma_i \propto -\omega_i^{-2}$. Increasing the value of ω_i^2 will reduce the magnitude of γ_i. Since by this definition – and as found in this study (Figure 5) – the low-frequency modes provide the largest negative contribution to the overall $\overline{\gamma}$. Simply allowing a small increase to the calculated frequencies of the low frequency RUMs in Si(NCN)$_2$, and we note that the values we calculated through expansion of the unit cell are certainly affected by our arbitrary value of our unit cell parameter. This sensitivity is reflected in the very large values of the mode Grüneisen parameters seen in Figure 5.

Another reason for a larger ω_i^{-2} and hence lower γ_i is from renormalisation through fourth-order phonon-phonon interactions, which must indeed exist and be strong enough to stabilise the cubic phase. We already know from previous work that these interactions reduce the size of the negative thermal expansion at higher temperatures [61].

However, more pertinent might be the comparison with the thermal expansion in β-cristobalite. This is a material that surely is expected to show NTE, but in truth show positive expansion over a wide temperature range [64] until finally showing NTE only at very high temperature [19]. β-cristobalite shows the same sort of RUM disorder we see in Si(NCN)$_2$ as discussed above. In the case of β-cristobalite, there is considerable thermal motion at all temperatures involving significant displacements of the oxygen atoms that are sufficiently anharmonic that a quasiharmonic description is not appropriate. That said, the quasiharmonic model and an interpretation based on the role of the RUMs appears to be appropriate [8, 38]. By contrast, the corresponding RUMs in Zn(CN)$_2$ are much higher in frequency, as we remarked, which means that the same sort of disorder will not be observed in this material, and thus Zn(CN)$_2$ has the thermal expansion as predicted by the quasiharmonic model [65].

6. Lattice dynamic basis of the α–β phase transition in Si(NCN)$_2$

As noted earlier, a calculation of the phonon dispersion curves of Si(NCN)$_2$ for the structure optimised at a notional pressure of 0 GPa gave negative eigenvalues. At this point we can remark that these were the eight RUMs, and they appeared to be unstable for all wave vectors along the main symmetry directions in reciprocal space. By increasing the cubic lattice parameter it was possible to make all eigenvalues positive. This leads to the question of which is the last phonon whose eigenvalue becomes positive on continued expansion, and whether this one might be the soft mode for the known displacive phase transition. However, on expansion the RUMs moved towards positive eigenvalues almost uniformly, with the last mode turning positive at an incommensurate wave vector. It appears to us that there is therefore likely to be a very complex phase space of all potential instabilities, associated with all RUMs across all wave vectors, and the energy differences will be smaller than the inherent accuracy of the DFT method.

7. Discussion

Our aim in this paper was to explore the origin of NTE in β-Si(NCN)$_2$ using calculations of phonons using conventional DFT methods. The key results that we obtained are

1. β-Si(NCN)$_2$ has a tight spectrum of RUMs, all at low-frequencies and at all wave vectors. The RUMs include the transverse acoustic modes over the frequency range 0–0.7 TGZ, with the two sets of optic-mode RUMs (the displacement and twist modes) being within a band of frequencies between 1.1–1.7 THz. The phonons that involve the distortions of the SiN_4 tetrahedra have significantly higher frequency, starting at around 6 THz.
2. The displacement and twist RUMS give a strong contribution to NTE, but we highlighted here also the importance of the acoustic modes. We note that the earlier paper on NTE in β-Si(NCN)$_2$ considered only the displacement optic-modes in their discussion, and not the twist mode or the acoustic mode. The acoustic RUMs are of equal importance to the optic RUMs. The important role of acoustic modes in giving rise to NTE has been noted by us in other systems recently [41, 42, 44].
3. The comparison with Zn(CN)$_2$ is particularly interesting give the close similarities between the two structures and hence of the RUM spectrum. In both cases the acoustic RUMs are very important for NTE, but in Zn(CN)$_2$ the strong angular forces mean that the Zn–cyanide–Zn linkages are much more rigid than the Si–carbodiidime–Si linkage. This pushes the optic RUMs to higher frequencies in Zn(CN)$_2$, whereas in Si(NCN)$_2$ the linkage crumples easily. Indeed, all RUMs of the equilibrium structure are unstable, as they would be in a calculation of phonon dispersion curves for the analogous β-cristobalite [8], reflecting the lack of resistance against a transition to a phase of lower symmetry.
4. The fact that the interatomic distances in the crystal structure are significantly lower than predicted by DFT suggests a lot of dynamic disorder, analogous that seen in β-cristobalite and in this sense different from Zn(CN)$_2$. This is consistent with the spectrum of low-frequency RUMs.
5. The calculations within the quasi-harmonic model significantly over-estimates the size of the NTE. This may be associated with the fact that the relevant phonon frequencies are lower than they should be, either because of the arbitrary expansion of the lattice required to make the RUMs stable is not quite right, or because of phonon-phonon anharmonic interactions, but probably it is an effect of the dynamic disorder. We note that β-cristobalite, whose crystal structure and RUM spectrum would indicate that this material should have significant NTE, nevertheless has positive thermal expansion until high temperature.

8. References

[1] A W Sleight. Compounds that contract on heating. *Inorganic Chemistry*, 37(12):2854–2860, June 1998.

[2] John S O Evans. Negative thermal expansion materials. *Journal of the Chemical Society, Dalton Transactions*, (19):3317–3326, 1999.

[3] G D Barrera, JAO Bruno, THK Barron, and N L Allan. Negative thermal expansion. *Journal of Physics: Condensed Matter*, 17(4):R217–R252, 2005.

[4] W Miller, C W Smith, D S Mackenzie, and K E Evans. Negative thermal expansion: a review. *Journal of Materials Science*, 44(20):5441–5451, July 2009.

[5] Cora Lind. Two Decades of Negative Thermal Expansion Research: Where Do We Stand? *Materials*, 5(12):1125–1154, December 2012.

[6] C P Romao, K J Miller, C A Whitman, M A White, and B A Marinkovic. Negative thermal expansion (thermomiotic) materials. In *Comprehensive Inorganic Chemistry II: From elements to applications*, pages 127–151. Elsevier, 2013.

[7] Jun Chen, Lei Hu, Jinxia Deng, and Xianran Xing. Negative thermal expansion in functional materials: controllable thermal expansion by chemical modifications. *Chemical Society Reviews*, 44:3522–3567, May 2015.

[8] Martin T Dove and Hong Fang. Negative thermal expansion and associated anomalous physical properties: review of the lattice dynamics theoretical foundation. *Reports on Progress in Physics*, 79:066503, May 2016.

[9] R Mittal, M K Gupta, and S L Chaplot. Phonons and anomalous thermal expansion behaviour in crystalline solids. *Progress in Materials Science*, 92:360–445, March 2018.

[10] Charles Martinek and F A Hummel. Linear thermal expansion of three tungstates. *Journal of the American Ceramic Society*, 51:227–228, 1968.

[11] T A Mary, J S O Evans, T Vogt, and A W Sleight. Negative thermal expansion from 0.3 to 1050 Kelvin in ZrW_2O_8. *Science*, 272(5258):90–92, April 1996.

[12] J W Couves, R H Jones, S C Parker, P Tschaufeser, and C R A Catlow. Experimental verification of a predicted negative thermal expansivity of crystalline zeolites. *Journal of Physics: Condensed Matter*, 5(27):L329–L332, 1993.

[13] P Tschaufeser and S C Parker. Thermal expansion behavior of zeolites and $AlPO_4$s. *The Journal of Physical Chemistry*, 99(26):10609–10615, June 1995.

[14] Martin P Attfield and Arthur W Sleight. Strong negative thermal expansion in siliceous faujasite. *Chemical Communications*, (5):601–602, 1998.

[15] Martin P Attfield and Arthur W Sleight. Exceptional negative thermal expansion in $AlPO_4$-17. *Chemistry of Materials*, 10(7):2013–2019, July 1998.

[16] David A Woodcock, Philip Lightfoot, Luis A Villaescusa, Maria-Jose Díaz-Cabañas, Miguel A Camblor, and Dennis Engberg. Negative thermal expansion in the siliceous zeolites chabazite and ITQ-4: A neutron powder diffraction study. *Chemistry of Materials*, 11(9):2508–2514, September 1999.

[17] David A Woodcock, Philip Lightfoot, Paul A Wright, Luis A Villaescusa, and Miguel A Camblor. Strong negative thermal expansion in the siliceous zeolites ITQ-1, ITQ-3 and SSZ-23. *Journal of Materials Chemistry*, 9(2):349–351, 1999.

[18] Philip Lightfoot, David A Woodcock, Martin J Maple, Luis A Villaescusa, and Paul A Wright. The widespread occurrence of negative thermal expansion in zeolites. *Journal of Materials Chemistry*, 11(1):212–216, 2001.

[19] Ekatarina Bourova and Pascal Richet. Quartz and cristobalite: high-temperature cell parameters and volumes of fusion. *Geophysical Research Letters*, 25(13):2333–2336, December 2012.

[20] P R L Welche, V Heine, and M T Dove. Negative thermal expansion in beta-quartz. *Physics and Chemistry of Minerals*, 26(1):63–77, November 1998.

[21] Ekatarina Bourova, Steven Parker, and Pascal Richet. Atomistic simulation of cristobalite at high temperature. *Physical Review B*, 62(18):12052–12061, November 2000.

[22] Benjamin K Greve, Kenneth L Martin, Peter L Lee, Peter J Chupas, Karena W Chapman, and Angus P Wilkinson. Pronounced negative thermal expansion from a simple structure: Cubic ScF_3. *Journal of the American Chemical Society*, 132(44):15496–15498, November 2010.

[23] Karena W Chapman, Peter J Chupas, and Cameron J Kepert. Compositional dependence of negative thermal expansion in the Prussian blue analogues $M^{II}Pt^{IV}(CN)_6$ (M = Mn, Fe, Co, Ni, Cu, Zn, Cd). *Journal of the American Chemical Society*, 128(21):7009–7014, May 2006.

[24] T Matsuda, J E Kim, K Ohoyama, and Y Moritomo. Universal thermal response of the Prussian blue lattice. *Physical Review B*, 79(17):172302–4, May 2009.

[25] S Adak, L L Daemen, and H Nakotte. Negative thermal expansion in the Prussian Blue analog $Zn_3[Fe(CN)_6]$ 2: X-ray diffraction and neutron vibrational studies. *Journal of Physics: Conference Series*, 251(1):012007, December 2010.

[26] Sourav Adak, Luke L Daemen, Monika Hartl, Darrick Williams, Jennifer Summerhill, and Heinz Nakotte. Thermal expansion in 3d-metal Prussian blue analogs – A survey study. *Journal of Solid State Chemistry*, 184(11):2854–2861, November 2011.

[27] Andrew L Goodwin and Cameron Kepert. Negative thermal expansion and low-frequency modes in cyanide-bridged framework materials. *Physical Review B*, 71(14):140301, April 2005.

[28] Karena W Chapman, Peter J Chupas, and Cameron J Kepert. Direct observation of a transverse vibrational mechanism for negative thermal expansion in $Zn(CN)_2$: an atomic pair distribution function analysis. *Journal of the American Chemical Society*, 127(44):15630–15636, November 2005.

[29] Andrew L Goodwin, Brendan J Kennedy, and Cameron J Kepert. Thermal expansion matching via framework flexibility in zinc dicyanometallates. *Journal of the American Chemical Society*, 131(18):6334–6335, May 2009.

[30] R Mittal, M Zbiri, H Schober, E Marelli, S J Hibble, A M Chippindale, and S L Chaplot. Relationship between phonons and thermal expansion in $Zn(CN)_2$ and $Ni(CN)_2$ from inelastic neutron scattering and *ab initio* calculations. *Physical Review B*, 83(2):024301, January 2011.

[31] Ralf Riedel, Axel Greiner, Gerhard Miehe, Wolfgang Dressler, Hartmut Fuess, Joachim Bill, and Fritz Aldinger. The First Crystalline Solids in the Ternary Si-C-N System. *Angewandte Chemie International Edition in English*, 36(6):603–606, April 1997.

[32] Ralf Riedel, Edwin Kroke, Axel Greiner, Andreas O Gabriel, Lutz Ruwisch, Jeffrey Nicolich, and Peter Kroll. Inorganic Solid-State Chemistry with Main Group Element Carbodiimides. *Chemistry of Materials*, 10(10):1–16, October 1998.

[33] Peter Kroll, Miria Andrade, Xuehua Yan, Emanuel Ionescu, Gerhard Miehe, and Ralf Riedel. Isotropic negative thermal expansion in β-$Si(NCN)_2$ and its origin. *The Journal of Physical Chemistry C*, 116(1):526–531, February 2012.

[34] Ilia Ponomarev and Peter Kroll. 29Si NMR Chemical Shifts in Crystalline and Amorphous Silicon Nitrides. *Materials*, 11(9):1646–16, September 2018.

[35] Ian Swainson and Martin T Dove. Low-frequency floppy modes in β-cristobalite. *Physical Review Letters*, 71(1):193–196, July 1993.

[36] Martin T Dove, David A Keen, Alex C Hannon, and Ian P Swainson. Direct measurement of the Si–O bond length and orientational disorder in the high-temperature phase of cristobalite. *Physics and Chemistry of Minerals*, 24(4):311–317, May 1997.

[37] Matthew G Tucker, Matthew P Squires, Martin T Dove, and David A Keen. Dynamic structural disorder in cristobalite: neutron total scattering measurement and reverse Monte Carlo modelling. *Journal of Physics: Condensed Matter*, 13(3):403–423, December 2000.

[38] Stephen A Wells, Martin T Dove, Matthew G Tucker, and Kostya Trachenko. Real-space rigid-unit-mode analysis of dynamic disorder in quartz, cristobalite and amorphous silica. *Journal of Physics: Condensed Matter*, 14(18):4645–4657, April 2002.

[39] Elizabeth R Cope and Martin T Dove. Evaluation of domain models for β-cristobalite from the pair distribution function. *Journal of Physics: Condensed Matter*, 22(12):125401–7, March 2010.

[40] Peter Kroll, Ralf Riedel, and Roald Hoffmann. Silylated carbodiimides in molecular and extended structures. *Physical Review B*, 60(5):3126–3139, August 1999.

[41] Leila H N Rimmer, Martin T Dove, Björn Winkler, Dan J Wilson, Keith Refson, and Andrew L Goodwin. Framework flexibility and the negative thermal expansion mechanism of copper(I)

oxide Cu_2O. *Physical Review B*, 89(21):214115, June 2014.

[42] Hong Fang, Martin T Dove, Leila H N Rimmer, and Alston J Misquitta. Simulation study of pressure and temperature dependence of the negative thermal expansion in $Zn(CN)_2$. *Physical Review B*, 88(10):104306, September 2013.

[43] Leila H N Rimmer and Martin T Dove. Simulation study of negative thermal expansion in yttrium tungstate $Y_2W_3O_{12}$. *Journal of Physics: Condensed Matter*, 27:185401, April 2015.

[44] Leila H N Rimmer, Martin T Dove, Andrew L Goodwin, and David C Palmer. Acoustic phonons and negative thermal expansion in MOF-5. *Physical Chemistry Chemical Physics*, 16(39):21144–21152, September 2014.

[45] A P Giddy, M T Dove, G S Pawley, and V Heine. The determination of rigid-unit modes as potential soft modes for displacive phase transitions in framework crystal structures. *Acta Crystallographica Section A Foundations of Crystallography*, 49(5):697–703, September 1993.

[46] Kenton D Hammonds, Martin T Dove, Andrew P Giddy, Volker Heine, and Bjoern Winkler. Rigid-unit phonon modes and structural phase transitions in framework silicates. *American Mineralogist*, 81(9-10):1057–1079, October 1996.

[47] Volker Heine, Patrick R L Welche, and Martin T Dove. Geometrical Origin and Theory of Negative Thermal Expansion in Framework Structures. *Journal of the American Ceramic Society*, 82(7):1793–1802, July 1999.

[48] Martin T Dove. Flexibility of network materials and the Rigid Unit Mode model: a personal perspective. *Philosophical Transactions of the Royal Society A: Mathematical, Physical and Engineering Sciences*, 377(2149):20180222–18, May 2019.

[49] Stewart J Clark, Matthew D Segall, Chris J Pickard, Phil J Hasnip, Matt I J Probert, Keith Refson, and Mike C Payne. First principles methods using CASTEP. *Zeitschrift für Kristallographie - Crystalline Materials*, 220(5/6):191–4, May 2005.

[50] John P Perdew, Kieron Burke, and Matthias Ernzerhof. Generalized Gradient Approximation Made Simple. *Physical Revew Letters*, 77(18):3865–3868, October 1996.

[51] John P Perdew, Kieron Burke, Matthias Ernzerhof, and R Ernstorfer. Generalized Gradient Approximation Made Simple [Phys. Rev. Lett. 77, 3865 (1996)]. *Physical Revew Letters*, 78(7):1396, February 1997.

[52] Hendrik J Monkhorst and James D Pack. Special points for Brillouin-zone integrations. *Physical Review B*, 13(12):5188–5192, June 1976.

[53] Stefano Baroni, Stefano de Gironcoli, and Andrea Dal Corso. Phonons and related crystal properties from density-functional perturbation theory. *Reviews of Modern Physics*, 73:515–562, July 2001.

[54] Keith Refson, Paul R Tulip, and Stewart J Clark. Variational density-functional perturbation theory for dielectrics and lattice dynamics. *Physical Review B*, 73(15):R4954–12, April 2006.

[55] Alex Corkett, Philipp Konze, and Richard Dronskowski. Synthesis, Crystal Structure, and Chemical-Bonding Analysis of $BaZn(NCN)_2$. *Inorganics*, 6(1):1–10, March 2018.

[56] Matthew G Tucker, Martin T Dove, and David A Keen. Simultaneous analysis of changes in long-range and short-range structural order at the displacive phase transition in quartz. *Journal of Physics: Condensed Matter*, 12(48):L723–L730, November 2000.

[57] M G Tucker, D A Keen, and M T Dove. A detailed structural characterization of quartz on heating through the α–β phase transition. *Mineralogical Magazine*, 65(4):489–507, August 2001.

[58] Olaf Reckeweg and Arndt Simon. Azides and Cyanamides – Similar and Yet Different. *Zeitschrift fur Naturforschung*, 58b:1097–1104, September 2003.

[59] Hong Fang, Anthony E Phillips, Martin T Dove, Matthew G Tucker, and Andrew L Goodwin. Temperature-dependent pressure-induced softening in $Zn(CN)_2$. *Physical Review B*, 88:144103, October 2013.

[60] Hong Fang and Martin T Dove. Pressure-induced softening as a common feature of framework structures with negative thermal expansion. *Physical Review B*, 87:214109, June 2013.

[61] Hong Fang, Martin T Dove, and Anthony E Phillips. Common origin of negative thermal expansion

and other exotic properties in ceramic and hybrid materials. *Physical Review B*, 89(21):214103, June 2014.

[62] Andrew L Goodwin. Rigid unit modes and intrinsic flexibility in linearly bridged framework structures. *Physical Review B*, 74(13):134302, October 2006.

[63] Martin T Dove, Alexandra K A Pryde, Volker Heine, and Kenton D Hammonds. Exotic distributions of rigid unit modes in the reciprocal spaces of framework aluminosilicates. *Journal of Physics: Condensed Matter*, 19(27):275209, June 2007.

[64] I P Swainson and M T Dove. On the thermal expansion of β-cristobalite. *Physics and Chemistry of Minerals*, 22:61–65, 1995.

[65] J Zwanziger. Phonon dispersion and Grüneisen parameters of zinc dicyanide and cadmium dicyanide from first principles: Origin of negative thermal expansion. *Physical Review B*, 76(5):052102, August 2007.